Electronic Supplementary Material (ESI) for Journal of Materials Chemistry C.

Supplemental Material

Unconventional stoichiometric two-dimensional potassium nitrides with anion-driven metallicity and superconductivity

Qiuping Yang[1], Ying Zhao[1], Xue Jiang[1*], Baotian Wang[2,3], and Jijun Zhao[1]

[1] *Key Laboratory of Materials Modification by Laser, Ion and Electron Beams (Ministry of Education), Dalian University of Technology, Dalian 116024, China*

[2] *Institute of High Energy Physics, Chinese Academy of Sciences, Beijing 100049, China*

[3] *Spallation Neutron Source Science Center, Dongguan 523803, China*

[*]Corresponding Author Email: jiangx@dlut.edu.cn

Index **Page**

Computational details

The structure search approach is based on a global minimization of free energy surfaces merging *ab initio* total-energy calculations as implemented in the CALYPSO code[1–3]. Searches are carried out to identify the most stable structures with stoichiometries of KN_x (x = 1-4) using simulation cell sizes of 1-4 formula units (f.u.) at 0 K and the considered pressures of 1 atm. In the first step, random symmetric structures are constructed in which atomic coordinates are generated by the crystallographic symmetry operations. Local optimizations using the VASP code[4,5] are done with the conjugate gradient method, and are deemed to be converged when the enthalpy changes become smaller than 1×10^{-5} eV per cell. The cut-off energy for the expansion of wavefunctions into plane waves is set to 400 eV in all structure searches, and a Monkhorst–Pack k-mesh with a maximum spacing of $2\pi \times 0.06$ Å^{-1}. After the first generation of structures is optimized 60% of the lowest lying structures are selected to construct the next generation by PSO (Particle Swarm Optimization). 40% of the structures in the new generation are randomly generated. A structure fingerprinting technique using a bond characterization matrix is applied to the generated structures, so that identical structures are strictly forbidden. This procedure significantly enhances the diversity of the structures, which is crucial for maintaining the efficiency of the global search. In most cases, structure search simulations for each calculation are stopped after generating 1000 ~ 1200 structures (e.g., about 20 ~ 30 generations).

To further analyze the structures with higher accuracy, we select a number of structures with lower total enthalpies and perform structural optimization using density functional theory (DFT) within the generalized gradient approximation (GGA) as implemented in the VASP code. The electron-ion interaction is described by using the all-electron projector augmented-wave (PAW) method[6] with $3s^2 3p^6 4s^1$ and $2s^2 2p^3$ valence electrons for K and N atoms, respectively. The cut-off energy for the expansion of wavefunctions into plane waves is set to 600 eV in all calculations, and a Monkhorst–Pack k-mesh[7] with a maximum spacing of $2\pi \times 0.03$ Å^{-1}. This usually

gives enthalpies well converged to within ~1 meV/atom. The calculated cohesive energies of the KN_x (x=1-4) monolayers with the following expression:

$$E_{coh}=(E_K+xE_N-E_{KNx})/(1+x),$$

Where E_K, E_N, and E_{KNx} denote the energy of a single K atom, a single N atom, and the KN_x (x=1-4) monolayer, respectively. To determine the dynamic stability of the predicted structures, phonon calculations are performed using the finite displacement approach[8] as implemented in the Phonopy code[9].

Based on the estimated elastic constants, obtained by the strain-energy method, we further explore the mechanical properties. The Young's modules $Y(\theta)$ and Poisson's ratio $\nu(\theta)$ along any direction (θ is the angle relative to the positive x-direction) are defined as

$$Y(\theta)=\frac{c_{11}c_{22}-c_{12}^{2}}{c_{11}s^4+c_{22}c^4+(\frac{c_{11}c_{22}-c_{12}^{2}}{c_{66}}-2c_{12})c^2s^2}$$

$$v(\theta)=\frac{c_{12}(c^4+s^4)-(c_{11}c_{22}-\frac{c_{11}c_{22}-c_{12}^{2}}{c_{66}})c^2s^2}{c_{11}s^4+c_{22}c^4+(\frac{c_{11}c_{22}-c_{12}^{2}}{c_{66}}-2c_{12})c^2s^2}$$

where c=cosθ and s=sinθ.

Fermi surface nesting function $\xi(\boldsymbol{q})$ is calculated through:

$$\xi(q)=\sum_{k,m,\mathrm{n}}\delta(\varepsilon_{kn}-\varepsilon_F)\delta(\varepsilon_{k+qm}-\varepsilon_F)$$

The electron-phonon coupling calculations are carried out with the density functional perturbation (linear response) theory as implemented in the QUANTUM ESPRESSO package[10,11]. We employ ultrasoft pseudopotentials with $3s^23p^64s^1$, and $2s^22p^4$ as valence electrons for K, and N atoms, respectively. The kinetic energy cutoff for wave-function expansion is chosen as 70 Ry. To reliably calculate electron-phonon coupling in metallic systems, we need to sample dense k-meshes for the electronic Brillouin zone integration and enough q-points for evaluating the average

contributions from the phonon modes: we have used a 12 × 12 × 1 *k*-mesh and 6 × 6 × 1 *q*-mesh for calculating the superconducting T_c of KN_2 monolayer:

$$T_c = \frac{\omega_{\log}}{1.2}\exp\left[-\frac{1.04(1+\lambda)}{\lambda-\mu^*(1+0.62\lambda)}\right]$$

Here, k_B is the Boltzmann constant and μ^* is the Coulomb pseudopotential ($\mu^* = 0.1$). The magnitude of the EPC $\lambda_{q,v}$ can be calculated by:

$$\lambda_{q,v} = \frac{\gamma_{q,v}}{\pi h N(E_F)\omega_{q,v}{}^2}$$

where $\gamma_{q,v}$ is the phonon linewidth, $N(E_F)$ is the electronic density of states at the Fermi level, and the $\omega_{q,v}$ is the phonon frequency. The phonon linewidths $\gamma_{q,v}$ can be estimated by

$$\gamma_{qv} = \frac{2\pi\omega_{qv}}{\Omega_{BZ}}\sum_{k,n,m}\left|g^{v}_{kn,k+qm}\right|^2\delta(\varepsilon_{kn}-\varepsilon_F)\delta(\varepsilon_{k+qm}-\varepsilon_F)$$

where $\left|g^{v}_{kn,k+qm}\right|$ is the electron-phonon matrix element between two electronic states with momenta k and k + q at the Fermi level.

$$\mathrm{g}^{v}_{kn,k+qm}(k,q) = \left(\frac{\mathrm{h}}{2M\omega_{q,v}}\right)^{\frac{1}{2}}\left\langle n,k\left|\delta V^{q,v}_{scf}\right|m,k+q\right\rangle$$

The Eliashberg spectral function for the electron-phonon interaction and the frequency-dependent EPC can be calculated by:

$$\alpha^2F(\omega) = \frac{1}{2\pi N(E_F)}\sum_{q,v}\frac{\gamma_{q,v}}{\omega_{q,v}}\delta(\omega-\omega_{q,v})$$

$$\lambda(\omega) = 2\int_0^{\omega}\frac{\alpha^2F(\omega)}{\omega}d\omega$$

$$\omega_{\log} = \exp\left[\frac{2}{\lambda}\int\frac{d\omega}{\omega}\alpha^2F(\omega)\ln(\omega)\right]$$

Anisotropic superconducting properties were investigated by solving the fully anisotropic Migdal-Eliashberg equations as implemented in the electron-phonon Wannier (EPW) code[12–14]. The precedent computations of the electronic wave functions required for the Wannier interpolations are performed in a uniform

unshifted BZ k-mesh of 12 × 12 × 1. An interpolated k-point grid of 120 × 120 × 1 and q-point grid of 120 × 120 ×1 are used to solve the anisotropic Migdal-Eliashberg equations. The fermion Matsubara frequencies cutoff is set to 0.6 eV, a reasonable setting is 3~4 times higher than the largest phonon frequency. The Morel-Anderson pseudopotential μ_c^* is set to 0.13.

Supplemental figures

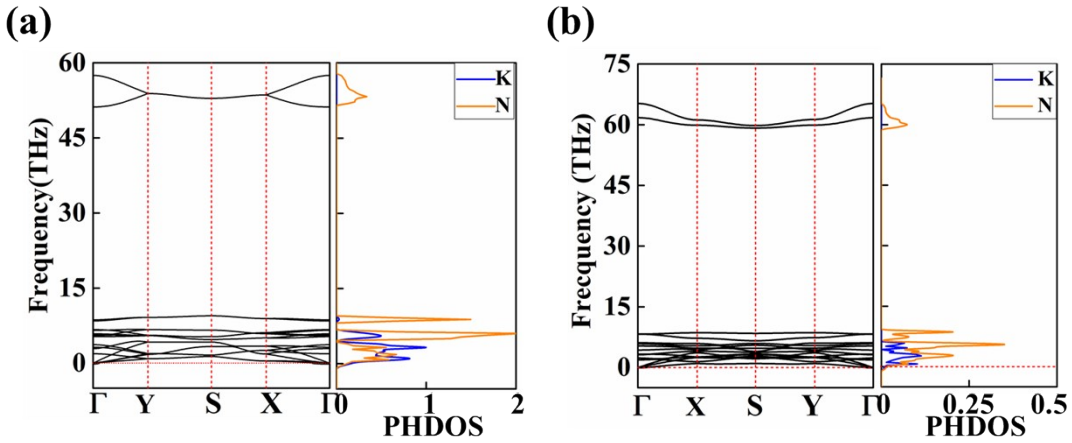

Figure S1. Phonon dispersion curves of (a) KN_2 and (b) KN_4 monolayers with unit-cell. The calculated phonon spectra indicate that the predicted KN_2 and KN_4 monolayers are all dynamically stable in view of absence of imaginary frequency modes in the first Brillouin zone.

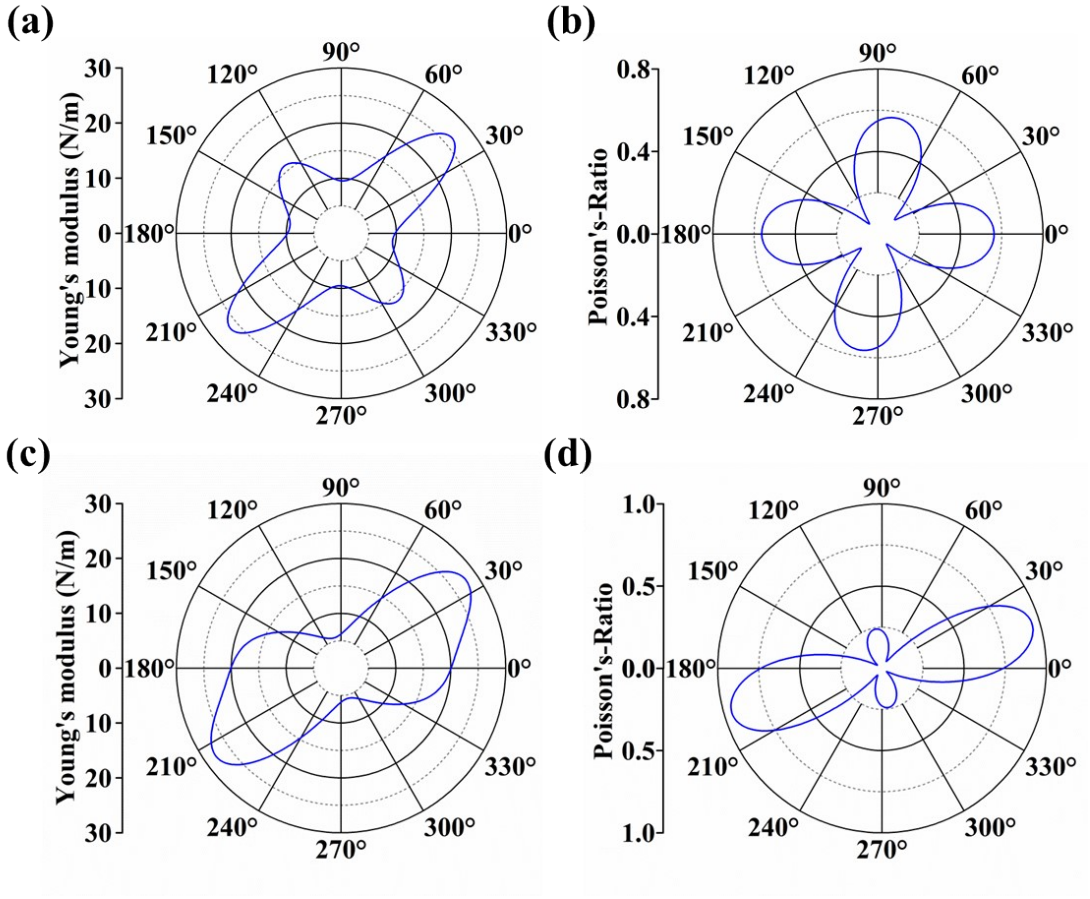

Figure S2. Direction dependences of Young's modulus and Poisson's ratio for (a, b) KN_2 and (c, d) KN_4 monolayers.

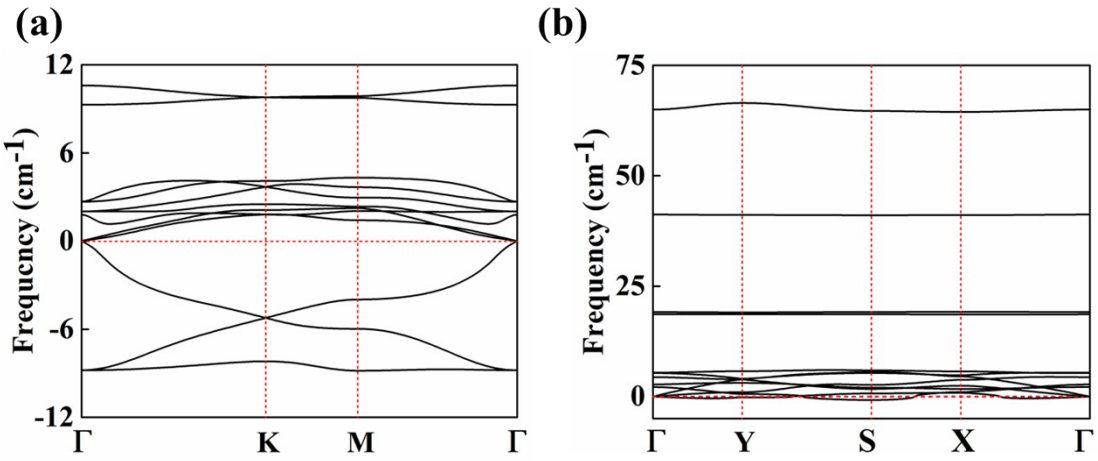

Figure S3. Phonon dispersion curves of predicted (a) KN and (b) KN_3 monolayers.

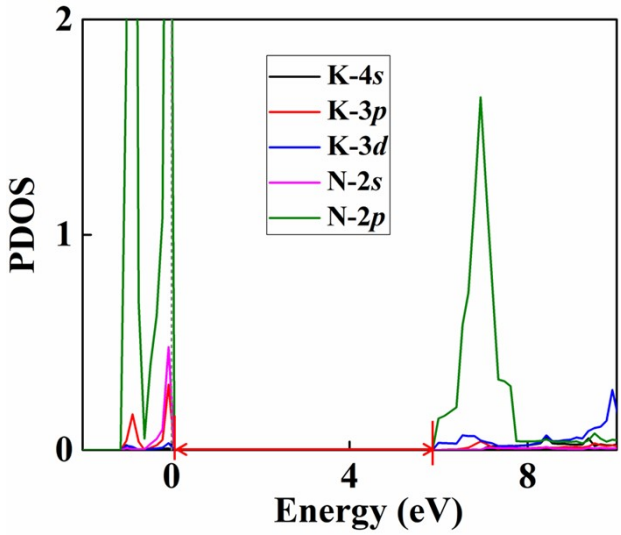

Figure S4. The projected density of states (PDOS) of the KN_2 monolayer doped with 1 hole/cell.

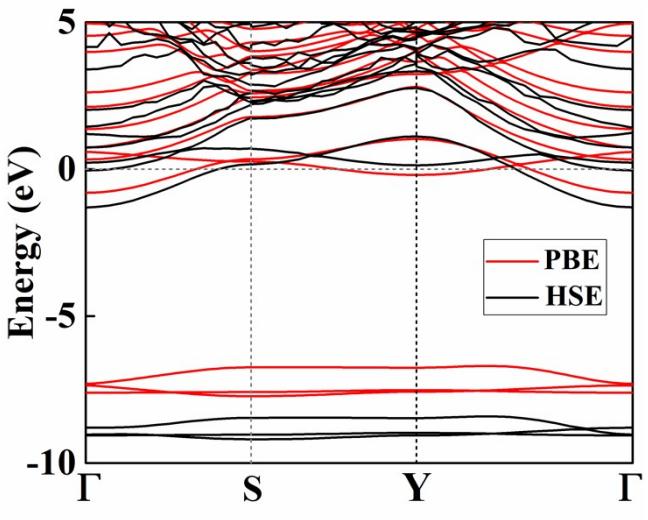

Figure S5. Electronic band structures of the KN_2 monolayer at the PBE (red) and HSE06 (black) levels.

Electronic properties for the KN_4 monolayer

To accurately describe the electronic properties of the KN_4 monolayer, we employ the PBE functional to calculate band structure and partial density of states (PDOS) (Figure S6). KN_4 is a metal with one band crossing the Fermi level. N 2*p* is more dominant component of the electronic states located near Fermi level.

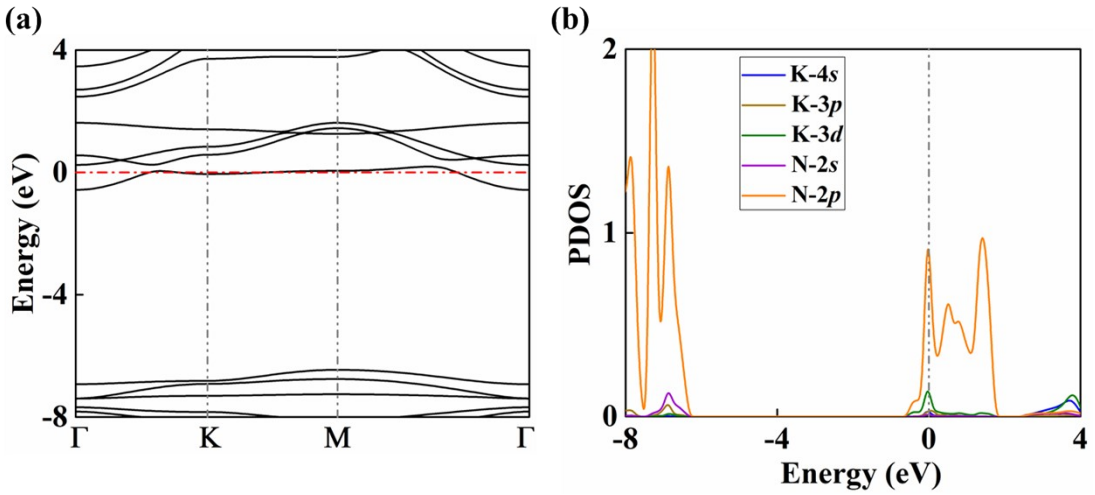

Figure S6. (a) Electronic band structure and (b) PDOS for KN_4 monolayer at the PBE level.

Supplemental tables

Table S1. The calculated values of elastic constants C_{ij} ($N*m^{-1}$) for the KN_2 and KN_4 monolayers at ambient pressure.

KN_2		KN_4	
C_{11}	15.521	C_{11}	26.610
C_{12}	8.354	C_{12}	7.821
C_{22}	14.036	C_{22}	9.608
C_{16}	3.657	C_{16}	4.343
C_{26}	1.591	C_{26}	4.017
C_{66}	9.684	C_{66}	7.560

According to the derived elastic constants (Table S1), the KN_2 and KN_4 monolayers satisfy the mechanical stability criteria $C_{11} > 0$, $C_{11}*C_{22}-C_{12}^2 > 0$ and $C_{66} > 0$.

Table S2. Bader atomic charge for KN_2 and KN_4.

Phases	Pressure	Atoms	Charge (e)
KN_2	1atm	K	0.82
		N1	-0.39
		N2	-0.42
KN_4	1atm	K	0.85
		N1	-0.20
		N2	-0.20
		N3	-0.20
		N4	-0.20

Table S3. Structural information for the stable K-N monolayers at the ambient pressure

Phases	Lattice Parameters (Å, °)	Wyckoff Positions (fractional)			
		Atoms	*x*	*y*	*z*
Cmmm-KN_2 primitive cell	*a* = 4.4278	K	-0.50000	0.50000	0.50000
	b = 4.4278	N	-0.91204	0.91204	0.50000
	c = 20.000				
	α = 90.0000				
	β = 90.0000				
	γ = 98.4442				
P-1-KN_4	*a* = 4.13700	K	1.00000	0.00000	0.50000
	b = 4.20420	N	0.60415	0.38357	0.58509
	c = 4.20420	N	0.58443	0.42977	0.41520
	α = 86.1606				
	β = 92.2621				
	γ = 94.1162				

References

1 Y. Wang, J. Lv, L. Zhu and Y. Ma, *Comput. Phys. Commun.*, 2012, **183**, 2063–2070.

2 Y. Wang, J. Lv, L. Zhu and Y. Ma, *Phys. Rev. B*, 2010, **82**, 94116.

3 B. Gao, P. Gao, S. Lu, J. Lv, Y. Wang and Y. Ma, *Sci. Bull.*, 2019, **64**, 301–309.

4 G. Kresse and J. Furthmüller, *Phys. Rev. B*, 1996, **54**, 11169–11186.

5 G. Kresse and D. Joubert, *Phys. Rev. B*, 1999, **59**, 1758–1775.

6 P. E. Blöchl, *Phys. Rev. B*, 1994, **50**, 17953–17979.

7 H. J. Monkhorst and J. D. Pack, *Phys. Rev. B*, 1976, **13**, 5188–5192.

8 K. Parlinski, Z. Q. Li and Y. Kawazoe, *Phys. Rev. Lett.*, 1997, **78**, 4063–4066.

9 A. Togo, F. Oba and I. Tanaka, *Phys. Rev. B*, 2008, **78**, 134106.

10 P. Giannozzi, S. Baroni, N. Bonini, M. Calandra, R. Car, C. Cavazzoni, D. Ceresoli, G. L. Chiarotti, M. Cococcioni, I. Dabo, A. Dal Corso, S. de Gironcoli, S. Fabris, G. Fratesi, R. Gebauer, U. Gerstmann, C. Gougoussis, A. Kokalj, M. Lazzeri, L. Martin-Samos, N. Marzari, F. Mauri, R. Mazzarello, S. Paolini, A. Pasquarello, L. Paulatto, C. Sbraccia, S. Scandolo, G. Sclauzero, A. P. Seitsonen, A. Smogunov, P. Umari and R. M. Wentzcovitch, *J. Phys. Condens. Matter*, 2009, **21**, 395502.

11 S. Baroni, S. de Gironcoli, A. Dal Corso and P. Giannozzi, *Rev. Mod. Phys.*, 2001, **73**, 515–562.

12 P. B. Allen and R. C. Dynes, *Phys. Rev. B*, 1975, **12**, 905–922.

13 A. B. Migdal, *Sov. Phys. JETP*, 1968, **35**, 996.

14 S. Poncé, E. R. Margine, C. Verdi and F. Giustino, *Comput. Phys. Commun.*, 2016, **209**, 116–133.